J Mater Sci (2009) 44:122–128
DOI 10.1007/s10853-008-3107-y

Sol-gel synthesis of alumina, titania and mixed alumina/titania in the ionic liquid 1-butyl-1-methylpyrrolidinium bis(trifluoromethylsulphonyl) amide

Hala K. Farag · Mohammad Al Zoubi · Frank Endres

Received: 7 September 2008 / Accepted: 7 November 2008 / Published online: 27 November 2008

Abstract In this paper we report on the synthesis of alumina, titania and mixed alumina–titania in the ionic liquid 1-butyl-1-methylpyrrolidinium bis(trifluoromethylsulphonyl) amide $[Py_{1,4}]TFSA$ via sol-gel methods using aluminium isopropoxide and titanium isopropoxide as precursors. Our results show that the as-synthesized alumina is mainly mesoporous boehmite with an average pore diameter of 3.8 nm. The obtained boehmite is subject to a phase transformation into γ-Al_2O_3 and δ-Al_2O_3 after calcinations at 800 and 1,000 °C, respectively. The as-synthesized TiO_2 shows amorphous behaviour and calcination at 400 °C yields anatase which undergoes a further transformation to rutile at 800 °C. The as-prepared alumina–titania powders are amorphous and transformed to rutile and α-Al_2O_3 after calcination at 1,000 °C TiO_2. The obtained alumina–titania has a higher surface area than those of alumina or titania. The surface area of the as-synthesized alumina–titania was found to exceed 486 $m^2\ g^{-1}$, whereas the surface areas of the as-synthesized boehmite and titania were around 100 $m^2\ g^{-1}$, respectively.

Introduction

Alumina, titania and their composite mixtures have a potential for applications as catalysts and support materials due to their specific properties such as thermal stability, high porosity and large surface area. Sol-gel methods are commonly used for the synthesis of such oxides involving the formation of an amorphous gel from a precursor solution. There are many studies on the synthesis of alumina [1–5], titania [6–8] and mixed alumina–titania [9–11] by sol-gel methods in organic solvents available in literature.

In recent times, there has been an increase of interest to use ionic liquids instead of organic solvents as reaction media for the synthesis of inorganic nanomaterials. Ionic liquids not only provide a usual environmentally benign media for many reactions but also catalyse some processes. In addition to the potential applications of ionic liquids as solvents, they are used as soft templates to synthesize nanostructured materials [12, 13]. Zhou and Antonietti [14] reported on the synthesis of crystalline TiO_2 nanoparticles in ionic liquids by hydrolysis of titanium tetrachloride in 1-butyl-3-methylimidazolium tetrafluoroborate (water-poor conditions) at 80 °C. The simplicity of the preparation method reflects the advantage of the use of ionic liquids since they facilitate direct synthesis of crystalline species under ambient conditions. Hence, there is no need for additives. Furthermore, ionic liquids can increase the nucleation rate by more than a factor of 1,000 as a result of their low interface tensions [15]. The high thermal stability of ionic liquids makes it possible to perform many reactions at temperatures of more than 100 °C in open cells. A large mesoporous nanostructured γ-Al_2O_3 was synthesized through a thermal process, at 120 °C, without postaddition of molecular or organic solvents in an open reaction vessel by using dual functions of the ionic liquid 1-hexadecl-3-methylimidazolium chloride $[C_{16}Mim]Cl$, i.e. having template and co-solvent functions [16]. The use of the ionic liquid $[BMIm]BF_4$ as template to prepare monolithic mesoporous silica via nanocasting was also reported [17]. Furthermore,

H. K. Farag · M. Al Zoubi · F. Endres (✉)
Institute of Particle Technology, Clausthal University of Technology, Robert-Koch-Str.42, 38678 Clausthal-Zellerfeld, Germany
e-mail: frank.endres@tu-clausthal.de

H. K. Farag
Inorganic Chemistry Department, National Research Centre, Dokki, Cairo, Egypt

nanosized TiO_2 particles with high surface area, controlled porosity and narrow pore size distribution were synthesized by a modified sol-gel method using the ionic liquid [BMIm]PF_6 [18, 19]. By addition of a surfactant as a pore templating material in sol-gel network, highly porous, thermally stable—up to 800 °C—anatase was obtained [18].

Quite recently we demonstrated the high potential of air and water stable ionic liquids for the synthesis of nanostructured alumina with very small grain sizes [20]. Different aluminium oxides were prepared by the hydrolysis of $AlCl_3$ dissolved in the ionic liquids 1-butyl-1-methylpyrrolidinium bis(trifluoromethylsulphonyl) amide ([$Py_{1,4}$] TFSA) and 1-ethyl-3-methylimidazolium bis(trifluoromethylsulphonyl) amide ([EMIm] TFSA), followed by calcinations. The procedure that we described is experimentally quite facile and delivers reproducibly different phases of nanostructured alumina. Furthermore, we showed that the employed ionic liquids can easily be recovered after the hydrolysis process [20]. This is due to the hydrolytic stability and the hydrophobicity of the TFSA anion. This result signifies the potential feasibility of employing air and water stable ionic liquids for sol-gel synthesis of nano-oxides without the usual problems of volatile organic compounds. We also reported the sol-gel synthesis of anatase and rutile, by hydrolysis of $TiCl_4$ in different ionic liquids [21]. A direct low temperature synthesis of rutile in the ionic [EMIm]TFSA was also described [22].

In the present work, sol-gel methods using aluminium isopropoxide and titanium isopropoxide precursors were employed for the synthesis of nanocrystalline alumina, titania and mixed alumina–titania in the ionic liquid [$Py_{1,4}$] TFSA. In our previous study on the synthesis of nano-alumina in ionic liquids, [$Py_{1,4}$] TFSA exhibited a templating effect, producing porous alumina with a high surface area [20]. Furthermore, we know from many other experiments that the $[Py_{1,4}]^+$ cation plays an important role in reducing the particle size since it adsorbs on the surface of nuclei preventing further growth. Therefore, we have employed the ionic liquid [$Py_{1,4}$]TFSA in the present work. The phase transformation obtained by calcinations of the synthesized oxides at variable temperatures was investigated by X-ray diffraction (XRD), thermogravimetric (TG) and differential thermal analysis (DTA). The surface morphology of the obtained nano-oxides was studied by a high-resolution scanning electron microscope (SEM) and the surface area was determined by BET (Brunauer-Emmett-Teller) measurements.

Experimental

Materials

The ionic liquid 1-butyl-1-methylpyrrolidinium bis(trifluoromethylsulphonyl) amide [$Py_{1,4}$]TFSA was purchased from Merck KGaA (EMD) in ultrapure quality. Aluminium isopropoxide ($Al(OPr\text{-}i)_3$) (Aldrich, 99.99%) and titanium isopropoxide ($Ti(OPr\text{-}i)_4$) (Aldrich 99.99%) were used without further purification as precursors for the synthesis of alumina and titania, respectively. Bi-distilled water was used to hydrolyse the precursor solutions. Acetone (Alfa 99.5%) was used for refluxing the obtained oxides. Preparation of solutions was carried out in an argon filled glove box with water and oxygen contents below 1 ppm (OMNI-LAB from Vacuum-Atmospheres).

Synthesis of alumina, titania and mixed alumina–titania

For alumina synthesis, a solution of 1 M $Al(OPr\text{-}i)_3$ in [$Py_{1,4}$]TFSA was prepared and then hydrolysed by dropwise addition of an appropriate amount of water. An emulsion was formed and then aged at 90 °C for about 12 h to form a gel under stirring. Afterwards, approximately a twofold volume of acetone was added into the reaction system and stirring maintained with refluxing at 50 °C for about 12 h. Then the mixture was centrifuged to reclaim the hydrolysis product. Finally, the hydrolysis product was left to dry in dry air for about 24 h, before calcinations.

The same procedure was employed for the synthesis of titania using 1 M $Ti(OPr\text{-}i)_4$ in [$Py_{1,4}$]TFSA. Alumina–titania was synthesized by co-hydrolysis of a mixture of 1 M $Al(OPr\text{-}i)_3$ and 1 M $Ti(OPr\text{-}i)_4$ in [$Py_{1,4}$]TFSA. The synthesized samples were calcined in a muffle oven at the desired temperature for 2 h and were cooled down to the ambient temperature in the oven.

Characterization

The morphology of the as-prepared and calcined products was investigated by means of a high-resolution field emission scanning electron microscope (Carl Zeiss DSM 982 Gemini). The phase compositions of the as-prepared and calcined products were analysed by X-ray diffraction (XRD) using a Siemens D-5000 diffractometer with CoK_α radiation. Thermogravimetric (TG) and differential thermal analysis (DTA) were carried out by a NETZSCH STA 409 PC thermal analyser at a heating rate of 10 °C/min starting from room temperature up to 1100 °C in air.

Nitrogen sorption results were obtained using a Quantachrome Autosorb-1 automated gas sorption analyser. Prior to the sorption measurements, the sample was degassed for 60 h at 150 °C under pressure of 100 μTorr. The surface area was calculated by the BET (Brunauer-Emmett-Teller) equation and the pore size was determined by the BJH (Barret-Joyner-Hallender) model.

Results and discussion

Synthesis of alumina

Figure 1 shows XRD patterns of as-synthesized and calcined samples. The as-synthesized alumina samples (boehmite) were calcined at 400, 800 and 1,000 °C. The different transition aluminas are χ, η, γ and ρ, in low temperature range (250–900 °C) and δ, κ and θ at higher temperatures [23]. α-alumina, usually known as corundum, is the end structure of transition aluminas formed at higher temperatures ($T \geq 1{,}000$ °C). During calcination the as-prepared samples appear grey in colour at 350 °C due to the presence of char residues as a result of the decomposition of the remaining ionic liquid. At a temperature of 650 °C the powder becomes fully white signifying the oxidation of char to volatile products. The thermal degradation of some important ionic liquids including TFSA-based liquids was reported by Scott and co-workers [24, 25].

As shown in Fig. 1, the XRD patterns of the as-synthesized sample exhibit broad peaks where aluminium oxyhydroxide AlO(OH), boehmite, has its main peaks. This means that crystalline boehmite is the primary product of $Al(OPr\text{-}i)_3$ hydrolysis in $[Py_{1,4}]TFSA$. The hydrolysis reaction can be expressed by the following equation:

$$Al(OPr\text{-}i)_3 + 2H_2O = AlOOH + 3i\text{-}PrOH \quad (1)$$

The broad peaks indicate the presence of very fine boehmite particles. The SEM micrograph of Fig. 2 shows the morphology of an as-synthesized boehmite sample. As can be seen, the sample contains very fine particles with sizes between 10–20 nm. At 400 °C, the prepared boehmite is thermally stable. Calcination of the boehmite

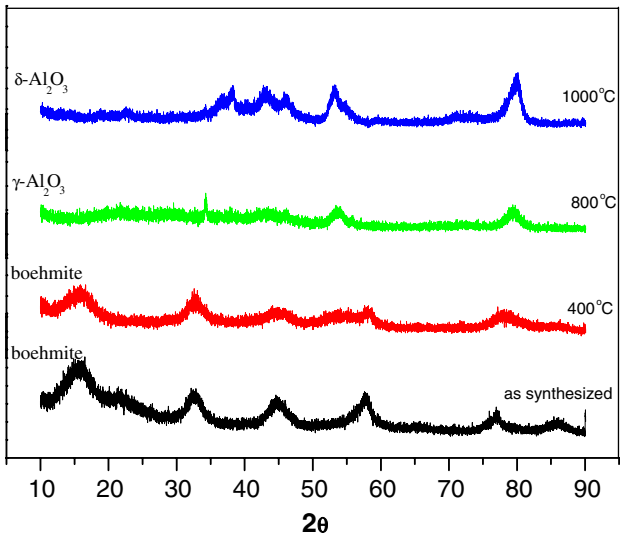

Fig. 1 XRD patterns of as-synthesized boehmite prepared in $[Py_{1,4}]TFSA$ containing 1 M $Al(OPr\text{-}i)_3$, without and with calcinations at different temperatures

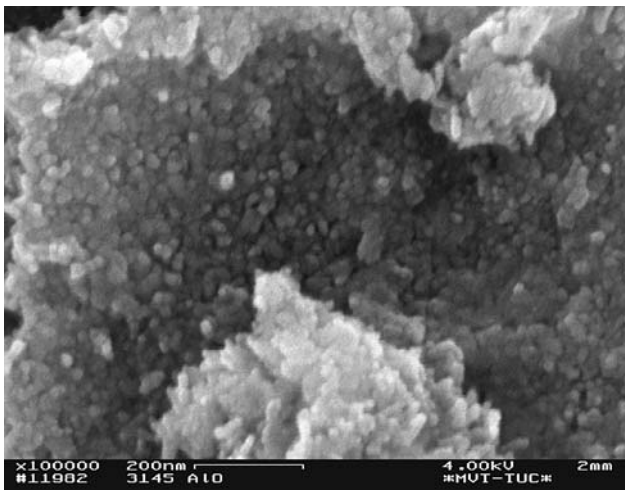

Fig. 2 SEM micrograph of the as-synthesized boehmite sample

phase at 800 °C leads to the formation of poorly crystalline γ-Al_2O_3. At 1,000 °C, γ-Al_2O_3 transforms to δ-Al_2O_3. The following equations describe the phase transformations during calcinations of the as-synthesized boehmite samples:

$$2AlOOH \xrightarrow{800\,^\circ C} \gamma\text{-}Al_2O_3 + H_2O \quad (2)$$

$$\gamma\text{-}Al_2O_3 \xrightarrow{1{,}000\,^\circ C} \delta\text{-}Al_2O_3 \quad (3)$$

Typical differential thermal analysis—thermogravimetric (DTA-TG) curves of the as-synthesized boehmite are shown in Fig. 3. The TG curve shows a gradual mass loss of about 15% in the temperature range of 35 to 300 °C and a large consecutive mass loss of about further 40% in the temperature range of 300–500 °C. The first mass loss is due to the evaporation of physically adsorbed water as well

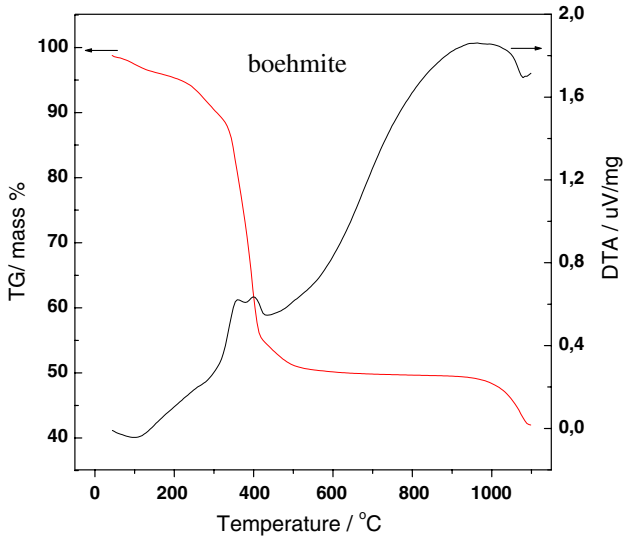

Fig. 3 DTA-TG curves of the as-synthesized boehmite sample

as of the residual organic solvent. As shown in the XRD patterns of Fig. 1, calcination of the sample up to 400 °C produces no change in the XRD patterns confirming that the lower temperature mass loss corresponds to adsorbed and not structural water of the boehmite phase. Three different processes might contribute to the observed high mass loss in the temperature range 300–500 °C: dehydration of chemisorbed water, dehydroxylation of AlOOH into γ-Al_2O_3 and decomposition or combustion of the residual ionic liquid. The observed higher temperature mass loss might be the result of the removal of the residual hydroxyls of the γ-phase [26, 27].

The DTA curve exhibits some endothermic and exothermic processes. The initial broad endotherm observed at about 100 °C is correlated to the evaporation of the adsorbed water in boehmite. Two small exotherms followed by a broad endotherm are recorded in the temperature range of 300 to 500 °C. The two exotherms could be attributed to the decomposition or combustion of the residual ionic liquid and the alkoxides residues. The recorded endotherm is attributable to the dehydroxylation of boehmite and formation of γ-Al_2O_3. Beyond the endotherm, an exothermic rise in the DTA curve up to a temperature of about 900 °C is observed as a result of the continued dehydroxylation reactions and crystallization of γ-Al_2O_3. The broad exotherm observed around 900–1,050 °C is correlated to the transformation from γ-Al_2O_3 to δ-Al_2O_3, as evidenced by the XRD results shown in Fig. 1.

Nitrogen adsorption–desorption isotherm measurements were carried out in order to determine the specific surface area, the porosity and the pore size distribution in the boehmite samples. As known, boehmite is widely used as a catalyst, especially for low temperature reactions. Furthermore, it is considered as a precursor for the preparation of catalyst supports and porous materials.

As manifested in Fig. 4, the nitrogen gas adsorption–desorption isotherm of the as-synthesized boehmite phase exhibits the typical IV behaviour for mesoporous materials. The adsorption–desorption curves overlap at low P/P^o range and then they begin to separate at $P/P^o \approx 0.4$ producing a pronounced hysteresis loop. This is attributable to capillary condensation in mesoporous materials. With further increase in P/P^o the capillary condensation ends and the two curves overlap again at $P/P^o \approx 0.8$. The flat part of the curves in the high P/P^o region is indicative of a narrow pore distribution in the prepared boehmite. The pore size distribution—obtained by Barret-Joyner-Hallender (BJH) model—of the prepared boehmite is shown in the inset of Fig. 4. As seen, the sample exhibits the typical characteristic of a mesoporous system with pore sizes around 3.8 nm. The prepared boehmite exhibits a specific surface area of 102 $m^2\ g^{-1}$, determined by Brunauer-Emmett-Teller (BET) equation.

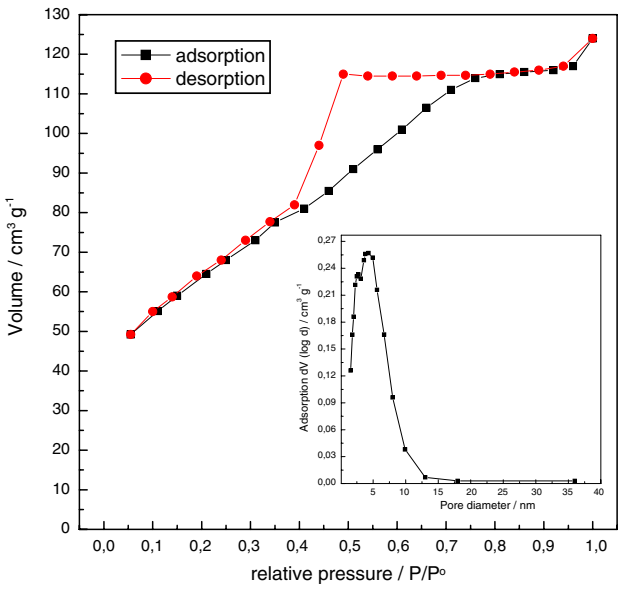

Fig. 4 Nitrogen gas adsorption–desorption isotherm of the boehmite phase obtained in $[Py_{1,4}]$TFSA containing 1 M $Al(OPr\text{-}i)_3$. Inset: pore size distribution

Synthesis of titania

There are three principle structural phases of titania, namely rutile, anatase and brookite. Rutile is the only stable phase, whereas anatase and brookite are metastable and transform to rutile on calcination. Anatase is the most widely used phase in catalysis and photocatalysis due to its higher surface area compared with other titania phases.

Titania was synthesized by hydrolysis of 1 M $Ti(OPr\text{-}i)_4$ in $[Py_{1,4}]$TFSA according to the following reaction:

$$Ti(OPr\text{-}i)_4 + 2H_2O = TiO_2 + 4i\text{-}PrOH \quad (4)$$

Figure 5 shows the XRD patterns of as-synthesized and calcined TiO_2 samples. The as-synthesized TiO_2 shows only a broad, very weak peak for anatase. This indicates the poor crystallization of the prepared titania. At 200 °C, there is no significant improvement in the crystallization although the main peak of anatase becomes a bit better pronounced. Calcination at 400 °C leads to a significant improvement in the crystallization of the anatase phase. The peaks are broad indicating the presence of very fine particles. At 600 °C, the anatase phase is still stable without any signals of the rutile phase. The phase transformation of TiO_2 from anatase, a phase with catalytic activity, to rutile usually occurs at 500–600 °C [28]. However, the prepared TiO_2 in the employed ionic liquid keeps its anatase structure after calcination at 600 °C for at least 2 h, as revealed in the XRD patterns (Fig. 5). This signifies that the prepared anatase is of high thermal stability, giving rise to applications as a catalyst, maybe over a wider temperature range. After calcination at

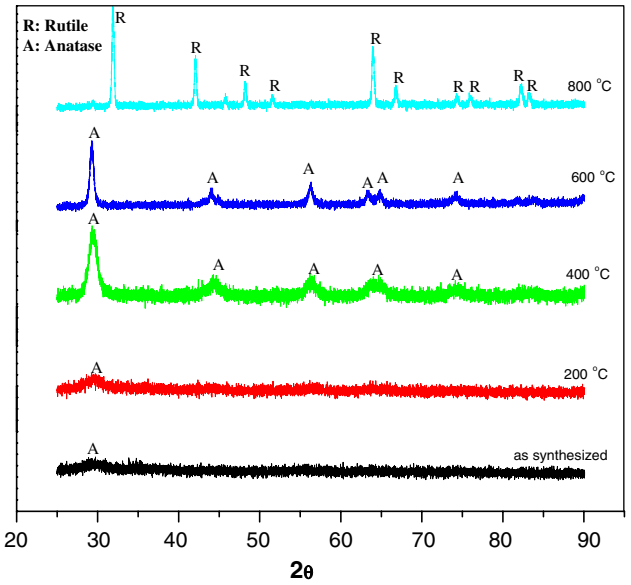

Fig. 5 XRD patterns of as-synthesized TiO_2 prepared in $[Py_{1,4}]TFSA$ containing 1 M $Ti(OPr\text{-}i)_4$, without and with calcinations at different temperatures

800 °C, the anatase phase is subject to a phase transformation into well crystallized rutile, Fig. 5. The BET surface area of the as-synthesized TiO_2 was found to be 97 $m^2\ g^{-1}$.

The DTA-TG curves of the prepared TiO_2 are displayed in Fig. 6. The TG curve can be roughly divided into three main processes. The highest mass loss (25%) is recorded in the temperature range from 35 to 150 °C, which can be ascribed to the evaporation of physically adsorbed water and the organic solvent. The second process is from 150 to 350 °C where a small mass loss of about 7% is observed as a result of the combustion of the remaining ionic liquid and organic residues. In the third process from 350 to 1,100 °C a mass loss of about 5% is observed. This might be attributable to the combustion of the ionic liquid residues and/or dehydration and evaporation of chemisorbed water [27].

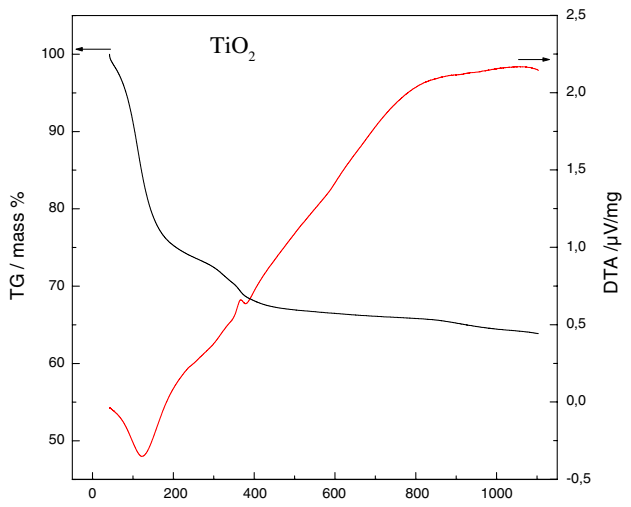

Fig. 6 DTA-TG curves of the as-synthesized TiO_2 sample

The DTA curve of Fig. 6 exhibits a pronounced endothermic peak at about 120 °C due to the evaporation of adsorbed water. A small exothermic peak observed at about 350 °C results from the thermal decomposition of the residual ionic liquid adsorbed by TiO_2. Then an exothermic rise in the DTA curve is recorded from 380 up to 800 °C. This could be ascribed to the crystallization of anatase, and after that the transformation of anatase to rutile occurs at about 800 °C, as shown in the XRD patterns of Fig. 5.

Synthesis of titania–alumina

Mixed alumina–titania oxides are widely used in catalysis as they exhibit properties superior to those of single-metal oxides (alumina or titania). For example, titanium oxide (anatase) is a good candidate as a catalyst, but it has the inconvenience of exhibiting—usually—a small surface area and, in some cases depending of the preparation method, poor structural stability at high temperatures. Aluminium oxides are more stable and have an acceptable surface area, but they have—usually—low catalytic activity. Therefore, mixed oxides were proposed to overcome the drawbacks of the single oxides.

An alumina–titania nano-particle mixture with a molar ratio of 1:1 was synthesized by the sol-gel method, during which the co-hydrolysis of equal molar concentrations of $Al(OPr\text{-}i)_3$ and $Ti(OPr\text{-}i)_4$ occurred. The as-synthesized product was calcined at different temperatures. Investigation of the crystalline phases formed during calcinations is of great importance for the application of the composite samples as catalysts or supports. This is due to the nature of the crystalline phase that can affect the catalytic behaviour of the catalyst.

Figure 7 shows the XRD patterns of the as-prepared and calcined titania–alumina samples. It is clearly seen that the as-prepared sample is amorphous. Also, the sample calcined at 400 °C shows amorphous behaviour, since no diffraction peaks are recorded. This might indicate that the mixed oxide contains very small crystallites to the extent that within the resolution of our XRD device no diffraction peaks could be obtained. This result is in agreement with the ones reported by Linacero et al. [29] for $x TiO_2$-$(1 - x)$ Al_2O_3 with $x \leq 0.6$, calcined at 500 °C for 3 h. They proposed that in these samples the titanium must be finely dispersed forming very small crystallites, whose sizes is not large enough to be detected by XRD [29]. Furthermore, Hirashima and co-workers [30] have reported that TiO_2/Al_2O_3 powders prepared by sol-gel methods in alcoholic solutions using metal alkoxides as precursors show amorphous behaviour at temperatures $\leq$750 °C.

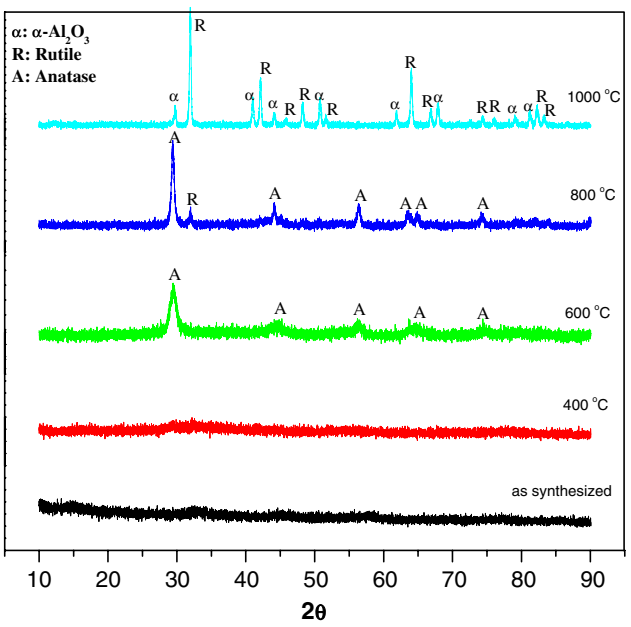

Fig. 7 XRD patterns of alumina–titania samples prepared in $[Py_{1,4}]TFSA$ containing 1 M $Al(OPr\text{-}i)_3$ and 1 M $Ti(OPr\text{-}i)_4$, without and with calcinations at different temperatures

Calcination at 600 °C yields the anatase diffraction peaks, and at 800 °C the diffraction peaks of anatase become more pronounced and trace amounts of rutile are also detected. Finally, after calcination at 1,000 °C the rutile phase and α-Al_2O_3 are observed. This suggests that during calcination the initially amorphous TiO_2 segregates and crystallizes into anatase then rutile prior to alumina formation. Interestingly, diffraction peaks of γ-Al_2O_3 or other metastable phases are not observed in any of the calcined samples. This finding was previously reported by Ramirez and Gutierrez-Alejandre [31]. They found that the incorporation of titania decreases the crystallinity of the γ-Al_2O_3 in such a way that the diffractograms of $x TiO_2$-$(1 - x)Al_2O_3$ samples with $x = 0.5$ and 0.7, calcined at 500 °C for 24 h, were amorphous. Another interesting phenomenon is that the anatase phase shows thermal stability up to a temperature of 800 °C. Thus, it can be concluded that the presence of alumina stabilizes the anatase phase and elevates the temperature at which the phase transformation to rutile occurs. This might enhance the activity of the prepared mixed oxide as a catalyst.

A thermogravimetric analysis, shown in Fig. 8, shows a pronounced weight loss (about 18%) in the low temperature region (35–150 °C) accompanied with an endothermic peak in the DTA curve due to the removal of adsorbed water from the sample. In the temperature range of 150 to 400 °C, another weight loss of about 16% (TG curve) and an exothermic peak (DTA curve) are recorded as a result of the combustion of the remaining ionic liquid and alkoxides residues. The observed exothermic rise of the DTA curve

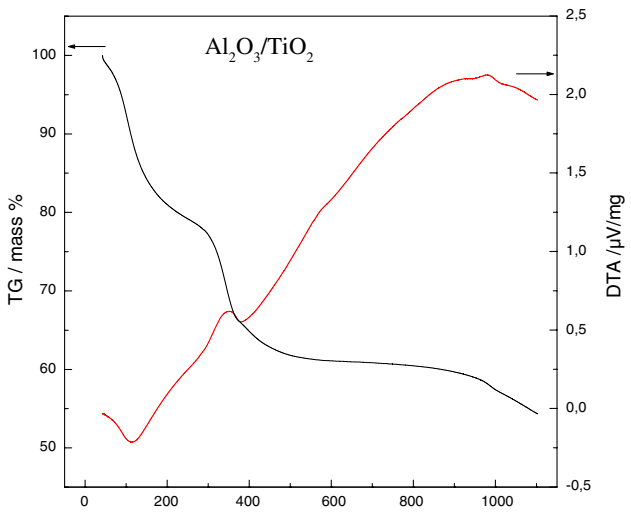

Fig. 8 DTA-TG curves of the as-synthesized alumina–titania sample

from 450 to 900 °C, as in the case of titania (Fig. 6) is correlated to the continued crystallization of the anatase phase. The XRD patterns show the formation of anatase at this temperature range (Fig. 7). After that, the crystallization of rutile and α-Al_2O_3 phases occur at temperatures of more than 800 °C, as indicated by the observed broad exotherm and the small exothermic peak, respectively (DTA curve). The recorded higher temperature weight loss in the TG curve could be attributed to the removal of the surface hydroxyls. Figure 9 shows a high-resolution SEM micrograph of as-synthesized alumina–titania. It is clearly seen that the particles are very fine with average sizes of about 10–20 nm.

Compared with the single boehmite and TiO_2, alumina–titania mixed oxide has a higher surface area. The surface area of the as-synthesized alumina–titania was found to exceed 486 $m^2\ g^{-1}$, whereas the surface areas of the as

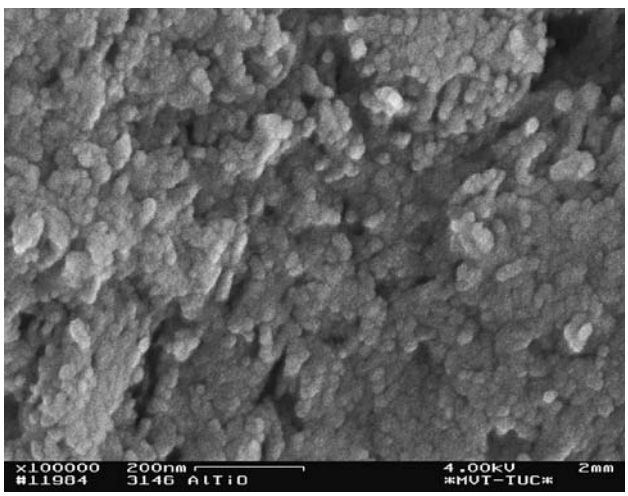

Fig. 9 SEM micrograph of the as-synthesized alumina–titania sample

synthesized boehmite and titania were less than 102 and 97 $m^2 g^{-1}$, respectively. This might give rise to a higher catalytic activity of the mixed oxide when it is employed as a catalyst. Further work is now under progress in our laboratories on improving the textural properties of the prepared single oxides by doping with nano-silver particles using plasmas as mechanically contact-free electrodes for the cathodic deposition of silver in $[Py_{1,4}]$TFSA. The aim is to improve the catalytic activity of the single oxides by Ag doping. Employing of plasma for electrodeposition of dispersed nano-Ag particles in ionic liquids was recently reported for the first time [32, 33].

The aforementioned results show that it is quite easy to produce in the ionic liquid $[Py_{1,4}]$TFSA Al_2O_3/TiO_2 powders with an active area of almost 500 $m^2 g^{-1}$. The ionic liquid synthesis of oxide nanoparticles does not require any additives—the nanoparticles form more or less naturally. The ionic liquids are non-volatile even at elevated temperatures, thus they are not evaporated and are not poisonous to the environment. Furthermore, the ionic liquids can easily be recovered after the synthesis of the nanoparticles and be reused for further syntheses. As there are also structure determining effects—as shown in literature—ionic liquids have due to their variety an enormous potential in the synthesis of metal oxide and mixed metal/metal oxide nanoparticles.

Conclusions

In the present paper alumina, titania and mixed alumina–titania with a molar ratio 1:1 were synthesized by sol-gel methods in $[Py_{1,4}]$TFSA using aluminium isopropoxide and titanium isopropoxide as precursors. Mesoporous boehmite with an average pore diameter of 3.8 nm was found to be the product of the hydrolysis of $Al(OPr\text{-}i)_3$ in $[Py_{1,4}]$TFSA. The obtained boehmite undergoes phase transformations into γ-Al_2O_3 and δ-Al_2O_3 after calcinations at 800 and 1,000 °C, respectively. The as-synthesized TiO_2 shows amorphous behaviour and calcination at 400 °C yields anatase which transforms to rutile at 800 °C. The as-prepared alumina–titania powders are amorphous and after calcination at 600 °C the TiO_2 anatase phase was observed, and at 1,000 °C rutile and α-Al_2O_3 were obtained. The presence of alumina in the mixed oxide results in stabilization of the anatase phase and elevation of the temperature at which the phase transformation to rutile occurs. The surface area of the as-synthesized alumina–titania was found to exceed 486 $m^2 g^{-1}$, whereas the surface areas of the as synthesized boehmite and titania were 102 and 97 $m^2 g^{-1}$, respectively.

Acknowledgement The authors would like to thank Prof. Dr Markus Antonietti, Max-Plank Institute, Potsdam, Germany, for gas sorption measurements and valuable advices.

References

1. Yoldas BE (1975) J Mater Sci 10:1856. doi:10.1007/BF00754473
2. Tsai MT, Shih HC (1993) J Mater Sci Lett 12:1025
3. Saha S (1994) J Sol-Gel Sci Technol 3:117
4. Le Bihan L, Dumeignil F, Payen E, Grimblot J (2002) J Sol-Gel Sci Technol 24:113
5. Park YK, Tadd EH, Zubris M, Tannenbaum R (2005) Mater Res Bull 40:1506
6. Reidy DJ, Holmes JD, Morris MA (2006) Ceram Int 32:235
7. Venkatachalam N, Palanichamy M, Murugesan V (2007) Mater Chem Phys 104:454
8. Qiu S, Kalita SJ (2006) Mat Sci Eng A 435–436:327
9. Kaneko EY, Pulcinelli SH, Teixeira da Silva V, Santilli CV (2002) Appl Catal A Gen 235:71
10. Jung Y-S, Kim D-W, Kim Y-S, Park EK, Baeck S-H (2008) J Phys Chem Solids 69:1464
11. Linacero R, Rojas-Cervantes ML, De D. Lopez-Gonzalez J (2000) J Mater Sci 35:3269. doi:10.1023/A:1004875322935
12. Firestone MA, Dietz ML, Seifert S, Trasobares S, Miller DJ, Zaluzec NJ (2005) Small 1:754
13. Liu Y, Wang M, Li Z, Liu H, He P, Li J (2005) Langmuir 21:1618
14. Zhou Y, Antonietti M (2003) J Am Chem Soc 125:14960
15. Antonietti M, Kuang D, Smarsly B, Zhou Y (2004) Angew Chem Int Ed 43:4988
16. Park H, Yang SH, Jun Y-S, Hong WH, Kang JK (2007) Chem Mater 19:535
17. Zhou Y, Schattka JH, Antonietti M (2004) Nano Lett 4:477
18. Choi H, Kim YJ, Varma RS, Dionysiou DD (2006) Chem Mater 18:5377
19. Yoo KS, Lee TG, Kim J (2005) Microporous Mesoporous Mater 84:211
20. Farag HK, Endres F (2008) J Mater Chem 18:442
21. Al Zoubi M, Farag HK, Endres F (2008) Aust J Chem 61:704
22. Kapper H, Endres F, Djerdj I, Antonietti M, Smarsly BM, Maier J, Hu Y-S (2007) Small 3:1753
23. Goodboy KP, Downing JC (1990) In: Hart LD (ed) Production, process, properties and applications of activated and catalytic aluminas. The American Ceramic Society Inc., Westerville, Ohio, p 93
24. Barayai KJ, Deacon GB, MacFarlane DR, Pringle JM, Scott JL (2004) Aust J Chem 57:145
25. Wooster TJ, Johanson KM, Fraser KJ, MacFarlane DR, Scott JL (2006) Green Chem 8:691
26. Mackenzie KJD, Temuujin J, Smith ME, Angeren P, Kameshima Y (2000) Thermochim Acta 359:87
27. Yu J, Zhao X, Zhao Q (2000) Thin Solid Films 379:7
28. Jing LQ, Sun XJ, Cai WM, Xu ZL, Du YG, Fu HG (2003) J Phys Chem Solids 64:615
29. Linacero R, Rojas-Cervantes ML, De D. Lopez-Gonzalez J (2000) J Mater Sci 35:3279. doi:10.1023/A:1004879507005
30. Tursiloadi S, Imai H, Hirashima H (2004) J Non-Cryst Solids 350:271
31. Ramirez J, Gutierez-Alejandre A (1997) J Catal 170:108
32. Meiss SA, Rohnke M, Kienle L, Zein El Abedin S, Endres F, Janek J (2007) ChemPhysChem 8:50
33. Zein El Abedin S, Pölleth M, Meiss SA, Janek J, Endres F (2007) Green Chem 9:549